Coastal Water Monitoring and Algorithm Development for Hyper-Spectrum Sensor

Ichio ASANUMA, Shinya Odagawa**, Chiaki Kobayashi**, Masaki Kawai**, Masatane Kato**, Genya Saitoh***, and Akihiro Kishima****

**The Tokyo University of Information Sciences, 1200-2, Yato, Wakaba, Chiba, Japan 265-8501*

***The Earth Remote Sensing Data Analysis Center, 3-12-1, Kachidoki, Chuo, Japan 104-0054*

****The University of Tohoku, 1-1, Tsutsumi, Amamiya, Aoba, Sendai, Japan 981-8555*

ABSTRACT

The airborne hyper-spectrum sensor was deployed over the coastal water to monitor bio-optical properties and to develop algorithms to estimate chlorophyll-a concentration, diffuse attenuation coefficient, and colored dissolved organic matter. The hyper-spectrum data will cover the missing information among bands, which are spectrum bands in the traditional satellite borne ocean color remote sensors. The new concept of algorithms using hyper-spectrum information will be discussed for the apparent optical property (AOP) and the inherent optical property (IOP). The test study area includes the coastal water with high turbidity and clear water within a range, and includes biologically damaged coastal floor.

Keywords: hyperspectral imaging, ocean color, CDOM, Kd, chlorophyll

1. INTRODUCTION

In the history of the ocean color remote sensing, the coastal water is the further problem for the alogorthm development including atmospheric correction and/or bio-optical algorithm (Wang et al., 2007, Chami, 2007, O'Reilly et al., 1998). Especially, the colored dissolved organic matter (CDOM) and the suspended particles in the case II water are unavoidable substances to be analyzed so as to obtain the chlorophyll-a concentration from remotely sensed data (IOCCG, 2000). As the case II water, located along the coast or on the continental shelf, exhibits the none-zero upwelling radiance at the red or in the near infra-red bands, it is difficult to remove an atmospheric contribution from the upwelling radiance in the short visible bands like 400 and 500 nm. In contrast, the case I water with only phytoplankton exhibits the zero upwelling radiance in the long wavelength and the current atomospheric correction works very well to remove the atmospheric contribution in the short visible bands. The accuracy of the atmospheric correction restricts the accuracy in the bio-optical algorithm combining the bands in the short visible bands.

Although, there remains an uncertainity in the atmospheric correction in the short visible bands over the case II waters, the bio-optical algorithms were porposed to estimate chlorophyll-a concentration, the CDOM, and the diffused attenuation coefficient at 490 nm (Kd490), where

Kd490 is used to represent the concentration of suspended particles. The chlorophyll-a concentration, CDOM and Kd490 are given by the empirical functions with the ratios among bands, but with the uncertainity in the coastal water. Sometimes, by the exceeding atmospheric correction from red and infra-red bands to the green and blue bands, the negative radiances are observed in the blue and green bands with resulting failers in estimating chlorophyll-a concentration and so on. Among ocean color scientists, there were many efforts to obtain the accurate bio-optical parameters from surface radiances (Siegel et al., 2002, Johannessen et al., 2003, Oliver et al., 2004). Unfortunately, the current discreate bands in the visible and near infra-red restrict the algorithm development to estimate chlorophyll-a, CDOM, and Kd490.

Recently, the hyperspectral imaging system has been implemented to the monitoring of land resources. Kerekes and Baum (2003) proposed the model for the hyperspectral imaging system to forecast remote sensing performance. The hyperspectral images were applied to many field of land remote sensing to identify and classify land objects (Mahesh and Mather, 2003, Haboudane et al., 2004, Thenkabail et al., 2004). Shafri et al. (2007) studied the performance of classification methods for the hyperspectral imaging data among the maximum likelihood classification, the spectral angle mapper, the nural network, and the decision tree classifiers. Plaza (2006) discussed the possibility of the parallel processing for the hyperspectral imaging. These land applications are intended to classify targets and slightly different from the application in the oceanography.

In advance to the application of the hyperspectral sensor to the oceanography, the atmospheric correction was proposed with a spectrum-matching technique (Gao et al., 2000). Base on these studies, the ocean Portable Hyperspectral Image for Low-Light Spectroscopy (ocean PHILLS) was developed and demonstrated a good spectrum measurements as well as in-situ measurements (Davis et al., 2002). The hyperspectral sensors are applied to the coastal region to monitor the benthic habitats (Dierssen et al., 2003, Filippi et al., 2006), and to the coral reef (Mishra et at., 2007). In the oceanography, the coastal water is the strong interest to be studied, because of their sensitivity to the environmental change on the land and human activities like the dam construction in the upstream region of rivers. The coastal water shoud be analyzed from the remote sensor with discreminating substances in the water.

In this study, we discuss a possibility to estimate CDOM as the inherent optical properties as a function of the aparent optical properties from the hyperspectral imaging data. We introduce the in-situ measurements including CTD profiling, water sampling, and following water analysis, which are conducted simultanously with the flight and measurements by the airborne hyperspectrum sensor near Japan.

2. METHOD FOR ALGORITHM DEVELOPMENT

2.1 CTD profiling with PAR sensor

The conductivity, tempeature and depth sensors (CTD, RBR-420) with the photo-synthetically available radiation (PAR) sensor are deployed from a small boat to get the vertical profile of water temperature, salinity, and PAR. This profiler is operated in a logger mode, and data are retrieved after the cruise. The PAR sensor gives the downwelling irradiance integrated from 400 to 700 nm. The profiles given by CTD will provide us the basic physical concept of the water column.

2.2 Irradiance and radiance measurements with on-board spectrum meter

The spectrum irradiance and radiance radiometers (TRIOS) are operated to measure the downwelling irradiance and the surface upwelling radiance with the above water measurement protocol (Hooker and Lazin, 2000). The spectrum coverage of these radiometers are from 350 to 900 nm. Also, the spectrum irradiance radiometer is deployed into the water column to estimate the diffused attenuation coefficient (Kd(λ)) from the downwelling irradiance measurement at two different depths. The diffused attenuation coefficient at 490 nm is reffered as one parameter to represent the concentration of suspended particles, which absorb and scatter the light penetration in the water column.

2.3 Water sampling

The surface water is sampled with a bucket sampling and the water near the bottom or at 10 m is sampled with the Niskin water sampler. The sampled water is analyzed to know the chlorophyll-a concentration, the nutrients concentration, the CDOM, and the suspended particles.

The chlorophyll-a concentration is determined by the fluorometric determination (Welschmeyer, 1994). The sampled sea water is filtered by the GF/F glass fiber filter. The GF/F filter is soaked with N, N-dimethylformamide for more than 24 hours. The fluorescence of the soaking liquid is measured by the Turner AU-10 to detemine the chlorophyll-a concentration.

A large portion of the CDOM is considered as the terrestrially derived dissolved organic carbon that enters the ocean and some portion of the CDOM is from the fate of phytoplankton and zooplankton in the ocean. As the CDOM is defined by the spectrum absorption at 300 nm, the CDOM exhibits a distinct absorption at the ultra-violet (UV) spectrum. The UV light from the solar irradiation has a function to inhibits a photosynthesis or to destroy the phytoplankton cell in the water. The UV penetration along the water column varies with the concentration of CDOM in the water. The sampled water is measured by the absorption spectrophotometer with 10 cm optical cell from 300 to 800 nm.

Suspended particles within the water are partly inorganic particles from river or ocean floor and organic particles from biogenic activities in the ocean. The chemical comsition of suspended particles vary and its optical properties also different in region. In this study, the sea water is filtered by the membran filter with a pore size of 0.2 μm and its dry weight is computed as the concentration of suspended particles in the unit volume. The concentration of suspended particles is compared with the diffused attenuation coefficient at 490 nm.

2.4 Hyperspectrum sensor measurements

The Airborne Imaging Spectrometer for Applications (AISA) is deployed synchronously with the in-situ measurement. The visible and near infrared sensor called Eagle and the short wave infrared sensor called Hawk are concurrently operated to get the surface radiance from 400 to 2400 nm with 190 channels.

The AISA data are processed for the atmospheric correction by the Fast Line-of-Sight Atmospheric Analysis of Spectral Hyercubes (FLAASH) to estimate the water leaving radiance.

3 DISCUSSION

The Sea Wide Field-of-View Sensor (SeaWiFS) and the Moderate Image Scanning Radiometer (MODIS), which have been used for ocean color monitoring, have the discrete spectrum bands, where a limited combination of spectrum bands are applied to estimate the concentrations of water substances. In contrast, the hyperspectrum sensor provides a continuous spectrum observation in all spectrum region with including a possibility to estimate geophysical parameters in different ways from the traditional ocean color algorithms.

Currently, the inherent optical properties like CDOM or Kd490 are estimated from the limitted number of apparent optical properties. Johannessen et al. (2003) proposed the empirical equation to estiamte the diffused attenuation coefficient at 323 nm, Kd(323), as follows;

$$K_d(323) = 0.781[R_{rs}(412)/R_{rs}(555)]^{-1.07} \quad (1)$$

where Rrs is the remote sensing reflectance that is given from the direct measurement of the remote sensor and the extrateristrial solar irradiation. Then, the spectral absorption coefficient of CDOM, $a_{CDOM}(323)$, is given by;

$$a_{CDOM}(323) = 0.904K_d(323) - 0.00714 \quad (2).$$

Simillary, Kd490 is given by the empirical equation (Mueller, 2000);

$$K_d(490) = 0.016 + 0.15645[{}_nL_w(490)/{}_nL_w(555)]^{1.5401} \quad (3)$$

These estimates of inherent optical properties from the apparent optical porperties have a freedom of 2 channels only.

In the hyperspectral remote sensing, we are able to increase the freedom of signal variation with more spectral bands. Fig. 1 shows the sample plots of three targets in 2007. One spectrum plot, showing a strong radiance in the near infra-red, is the upwelling radiance from the forest. Other two spectrum plots, exhibiting a low radiance in all spectrum range, are corresponding to the upwelling radiance from two different water mass.

We are currently, validating the hyperspectral data and in-situ data, and constracting a new algorithm to estimate an absorption coefficient for CDOM, a diffused attenuation coefficient of the water, and including chlorophyll-a concentration on the coastal waters.

The hyperspectrum remote sensing over the water is quite different from the target over lands, where the traditional classification does not work and it is required to classify the analogously distributed substances.

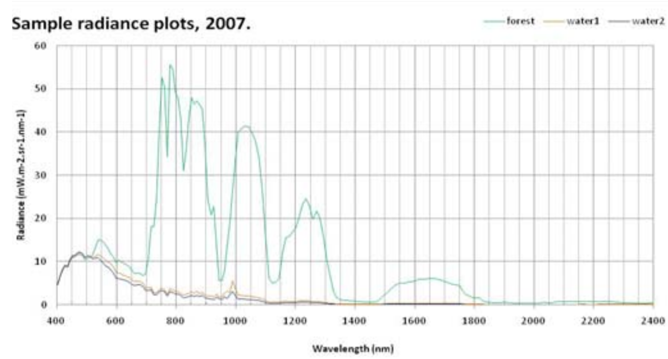

Fig. 1 Sample radiance plots from AISA 2007

REFERENCES

Chami, M. (2007), Importance of the polarization in the retrieval of oceanic constituents from the remote sensing reflectance, *J. G. R.,* 112, C05026, doi:10.1029/2006JC003843.

Davis, C. O., J. Bowles, R. A. Leathers, D. Korwan, T. V. Downes, W. A. Snyder, W. J.

Rhea, W. Chen, J. Fisher, W. P. Bissett, and R. A. Reisse (2002), Ocean PHILLS hyperspecral imager: design, characterization, and calibration, *Optics Express*, 10 (4), 210-221.

Dierssen H. M., R. C. Zimmerman, R. A. Leathers, T. V. Downes, and C. O. Davis (2003), Ocean color remote sensing of seagrass and bathymetry in the Bahamas Banks by high-resolution airborne imagery, *Limnol. Oceanogr.*, 48(1, part 2), 444-4555.

Filippi, A. M., K. L Carder, and C. O. Davis (2006), Vicarious calibration of the Ocean PHILLS hyperspectral sensor using a coastal tree-shadow method, *Geophys. Res. Lett.*, 33, L22605, doi:10.1029/2006GL027073.

Gao, B. C., M. J. Montes, Z. Ahmad, and C. O. Davis (2000), Atmospheric correction algorithm for hyperspectral remote sensing of ocean color from space, *Applied Optics*, 39 (6), 887-896.

Haboudane, D., J. R. Miller, E. Pattey, P. J. Zacro-Tejada, and I. Strachan (2004), Hyperspectral vegetation indices and novel algorithms for predicting green LAI of crop canopies: Modeling and validation in the context of precision agriculture, *Remote Sensing of Environment*, 90 (3): 337-352.

Hooker, S. B., and G. Lazin (2000), The SeaBOARR-99 Field Campaign, SeaWiFS Postlaunch Technical Report Series, NASA Tech Memo 2000-206892, 8, 46pp.

IOCCG (2000), Remote Sensing of Ocean Colour in Coastal, and Other Optically-Complex, Waters, Ed. S. Sathyendranath, 140pp.

Johannessen, S. C., W. L. Miller, and J. J. Cullen (2003), Calculation of UV attenuation and colored dissolved organic matter absorption spectra from measurements of ocean color, *J. G.. R.* 108(C9), 3301, doi:10.1029/2000JC000514.

Kerekes J. P. and J. E. Baum (2003), Hyperspectral Imaging System Modeling, Lincoln Laboratory Journal, 14, 1, 117-130.

Mahesh, P. and P. M. Mather (2003), An assessment of the effectiveness of decision tree methods for land cover classification, *Remote Sensing of Environment*, 86, 554-565.

Mishra, D. R., S. Narumalani, D. Rundquist, M. Lawson, and R. Perk (2007), Enhancing the detection and classification of coral reef and associated benthic habitats: A hyperspectral remote sensing approach, *J. Geophys. Res.*, 112, C08014, doi:10.1029/2006JC003892.

Mueller, J. (2000), SeaWiFS Algorithm for the Diffuse Attenuation Coefficient, K(490), Using Water-Leaving Radiances at 490 and 555 nm, *NASA Technical Memorandum* 2000-206892, (11), 24-27.

O'reilly, J. E., S. Maritorena, B. G. Mitchell, D. A. Siegel, K. L. Carder, S. A. Garver, M. Kahru, and C. McClain (1998), Ocean color chlorophyll algorithms for SeaWiFS, *J. Geophys. Res.,*103, C11, 24,937-24,953.

Oliver, M. J., O. Schofield, T. Bergmann, S. Glenn, C. Orrico. And M. Moline (2004), Deriving in situ phytoplankton absorption for bio-optical productivity models in turbid waters, *J. Geophys. Res.*, 109, C07S11, doi:10.1029/2002JC001627.

Plaza, A. (2006), Parallel processing opens new perspectives for hyperspectral imaging, *SPIE Newsroom*, 10.1117/2.1200606.0275.

Siegel, D. A., S. Maritorena, N. B. Nelson, D. A. Hansell, and M. Lorenzi-Kayser (2002), Global distribution and dynamics of colored dissolved and detrital organic materials, *J. Geophys. Res.*, 107(C12), 3228, doi:10.1029/2001JC000965.

Shafri, H. Z. M., A. Suhaili, and S. Mansor (2007), The Performance of Maximum Likelihood, Spectral Angle Mapper, Neural Network and Decision Tree Classifiers in Hyperspectral Image Analysis, *J. Computer Science*, 3 (6): 419-423.

Thenkabail, P. S., E. A. Enclona, M. S. Ashton, B. Van, D. Meer (2004), Accuracy assessments of hyperspectral waveband performance for vegetation analysis applications, *Remote Sensing of Environment*, 91 (3-4): 354-376.

Wang, M., J. Tang, and W. Shi (2007), MODIS-derived ocean color products along the China east coastal region, *Geo. Res. Lett.*, 34, L06611, doi:10.1029/2006GL028599

Welschmeyer, N. A. (1994), Fluorometric analysis of chlorophyll a in the presence of chlorophyll b and phaeopigments, *Limnol. Oceanogr.* 39, 1985-1992

Development of Mangrove Spectral Library

Hartanto Sanjaya, Ariani Andayani
Center for Natural Resources Inventory (TISDA), Agency for Assessment and Application of Technology (BPPT).
Institute of Marine Research and Observation, Research Center for Marine Technology (PRTK), Agency for Marine and Fisheries Research (BRKP), Ministry of Marine Affairs and Fisheries

Development of mangrove spectral library

Hartanto Sanjaya, Center for Natural Resources Inventory (TISDA), Agency for Assessment and Application of Technology (BPPT).

Ariani Andayani, Institute of Marine Research and Observation, Research Center for Marine Technology (PRTK), Agency for Marine and Fisheries Research (BRKP), Ministry of Marine Affairs and Fisheries

Presented on APEC SAKE Workshop, Jakarta, 5 November 2007

Methods

- Study Site and Survey Design
- Mangrove Identification
- Field Data Acquisition (Measurement Procedure)

- Introduction
- Methods
  - Study Site, and Survey Design
  - Mangrove Identification
  - Field Data Acquisition
- Result
- References

Method: Study Sites and Survey Design

- In September of 2007 reflectance spectra were collected in Mangrove areas, Southern part of Kabupaten Jembrana, Bali:
  - Perancak
  - Delod Brawah
  - Tuwed

Introduction

- Spectral Library => finger print of objects => remote sensing data analysis.
- Mangroves => important plants in coastal zones.
- This study is to develop spectral library of Mangroves species.

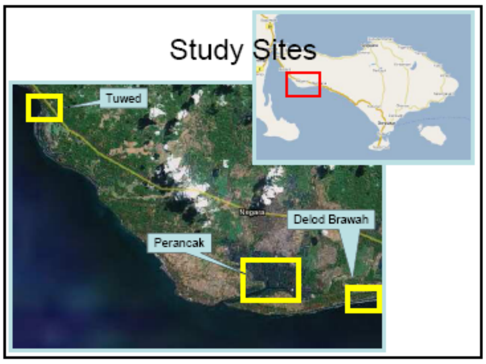

Method: Survey Design

- Survey Design:
  - mangrove mapping ("roughly")
    - identify the locations,
    - plan the optimum tracks
    - need special day(s)
  - Acquisition timing:
    - effective time range: 10am – 2pm
    - Number of days: depends

Method:
Field Data Acquisition

- Reference and dark spectrum must be measured if at any time any sampling variable changes.
- In order to remove random noise from the spectral reflectance, the three spectra collected for each sample were averaged.

Method: Mangrove Identification

- "keys" to identify mangrove species:
  - Roots
  - Leaves
  - Flowers and Fruits
  - Tree's shape
- Reference: Handbook of Mangroves

(in actions ☺…)

Tuwed, Jembrana, 2007

Mangrove Identification

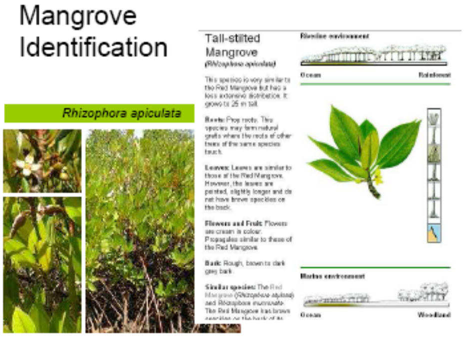

Result

- Perancak Estuary (13 species):
  - *Acanthus ilicifolius, Aegiceras corniculatum, Avicennia alba, Avicennia marina, Bruguiera gymnorrhiza, Ceriops decandra, Hibiscus tiliaceus, Nypa fruticans, Sonneratia alba, Excoecaria agalocha, Xylocarpus granatum, Rhizophora stylosa, Rhizophora apiculata*
- Delod Brawah (2 species):
  - *Pandanus tectorius, Scaevola tacada*
- Tuwed (6 species):
  - *Ceriops decandra, Ceriops tagal, Spinifex littoreus, Osbornia octodonta, Sonneratia alba, Thespesia populnea*

Method:
Field Data Acquisition

- For each tree, 3 spectral measurements were taken of the sunlit side of the tree, at nadir from a distance of approximately 10 - 20 cm using a USB2000 Ocean Optics field spectrometer, equipped with a fiber optic cable of 1.5m.

Rhizophora apiculata

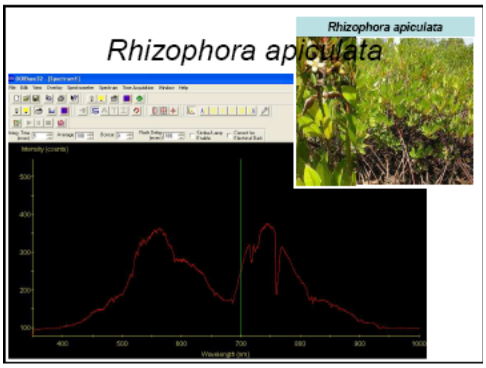

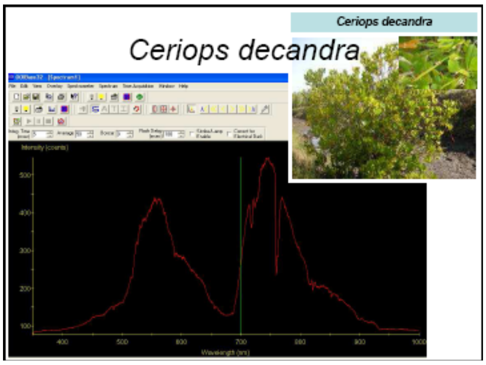

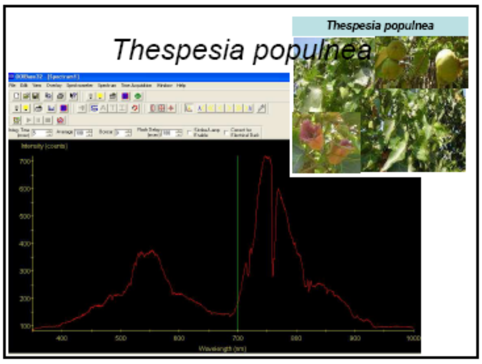

References

- **Ferwerda, et.al.**, 2002, *Field Spectrometry of Leaves for Nutrient Assessment*, ITC The Netherland.
- **Kitamura, Sozo et,al.**, 1997, *Handbook of Mangroves in Indonesia – Bali & Lombok*, Ministry of Forestry Indonesia, Japan International Cooperation Agency (JICA), The International Society of Mangrove Ecosystems (ISME), ISBN:4-906584-04-7.

Land Cover Classification of Fordata Island with Hyperspectral Data

MCG. Frederik, Y. Wahyudi, H. Sanjaya, M. Sadly, D. Yusuf, I. Farahidy
Center for Technology of Natural Resources Inventory (PTISDA)
Agency for Assessment and Application of Technology (BPPT)

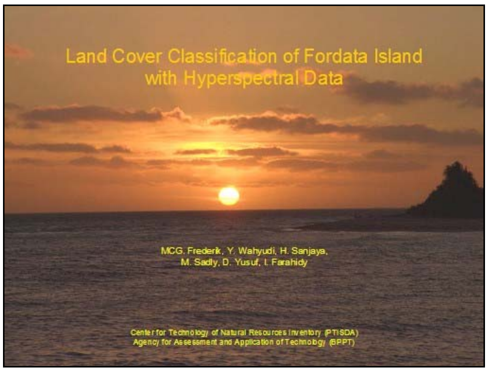

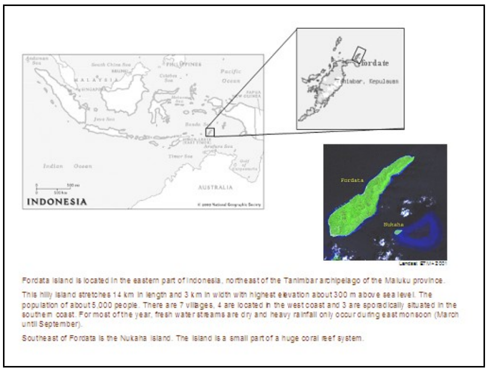

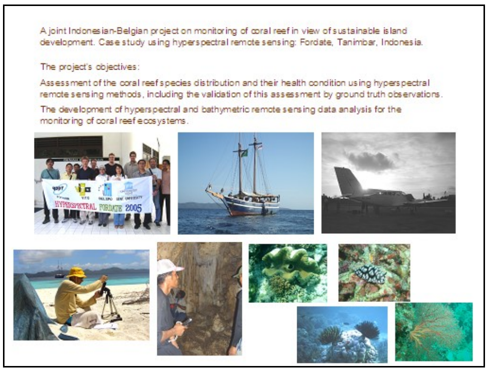

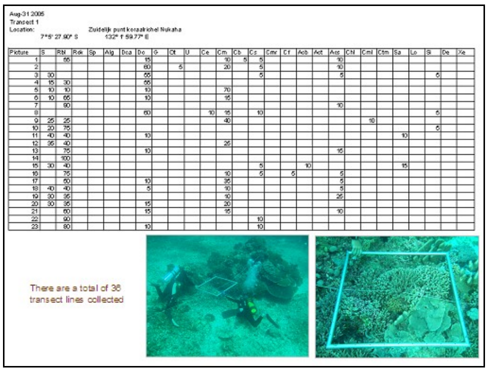

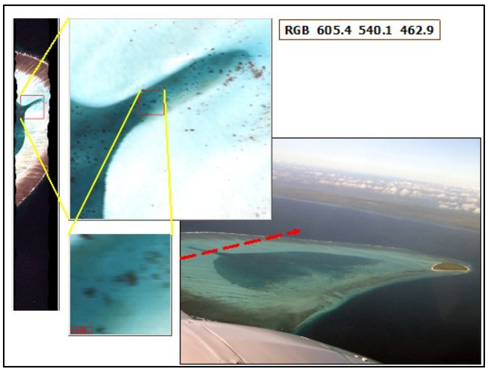
RGB 605.4 540.1 462.9

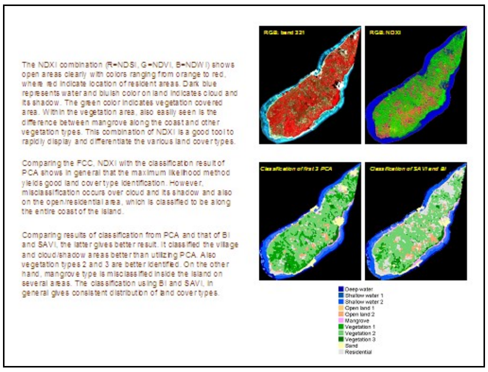
The NDXI combination (R=NDSI, G=NDVI, B=NDWI) shows open areas clearly with colors ranging from orange to red, where red indicate location of resident areas. Dark blue represents water and bluish color on land indicates cloud and its shadow. The green color indicates vegetation covered area. Within the vegetation area, also easily seen is the difference between mangrove along the coast and other vegetation types. This combination of NDXI is a good tool to rapidly display and differentiate the various land cover types.
Comparing the FCC, NDXI with the classification result of PCA shows in general that the maximum likelihood method yields good land cover type identification. However, misclassification occurs over cloud and its shadow and also on the open/residential area, which is classified to be along the entire coast of the island.
Comparing results of classification from PCA and that of BI and SAVI, the latter gives better result. It classified the village and cloud/shadow areas better than utilizing PCA. Also vegetation types 2 and 3 are better identified. On the other hand, mangrove type is misclassified inside the island on several areas. The classification using BI and SAVI, in general gives consistent distribution of land cover types.
RGB: band 321
RGB: NDXI
Classification of first 3 PCA
Classification of SAVI and BI
Deep water
Shallow water 1
Shallow water 2
Open land 1
Open land 2
Mangrove
Vegetation 1
Vegetation 2
Vegetation 3
Sand
Residential

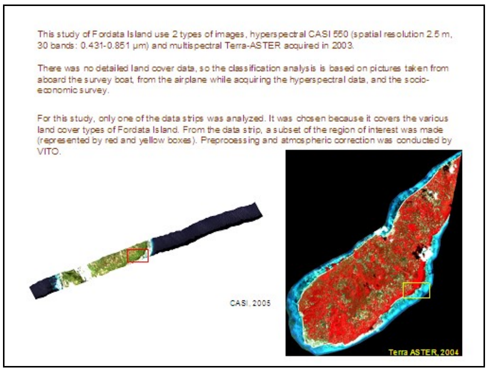
This study of Fordata Island use 2 types of images, hyperspectral CASI 550 (spatial resolution 2.5 m, 30 bands: 0.431-0.851 µm) and multispectral Terra-ASTER acquired in 2003.
There was no detailed land cover data, so the classification analysis is based on pictures taken from aboard the survey boat, from the airplane while acquiring the hyperspectral data, and the socio-economic survey.
For this study, only one of the data strips was analyzed. It was chosen because it covers the various land cover types of Fordata Island. From the data strip, a subset of the region of interest was made (represented by red and yellow boxes). Preprocessing and atmospheric correction was conducted by VITO.
CASI, 2005
Terra ASTER, 2004

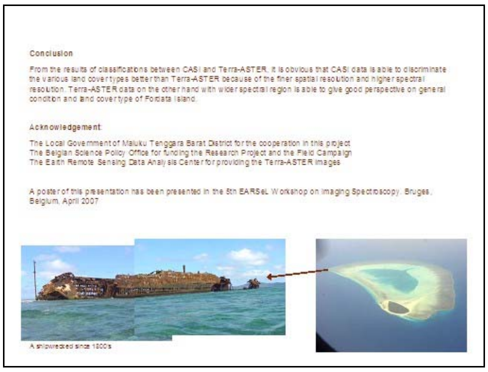
Conclusion
From the results of classifications between CASI and Terra-ASTER, it is obvious that CASI data is able to discriminate the various land cover types better than Terra-ASTER because of the finer spatial resolution and higher spectral resolution. Terra-ASTER data on the other hand with wider spectral region is able to give good perspective on general condition and land cover type of Fordata Island.
Acknowledgement:
The Local Government of Maluku Tenggara Barat District for the cooperation in this project
The Belgian Science Policy Office for funding the Research Project and the Field Campaign
The Earth Remote Sensing Data Analysis Center for providing the Terra-ASTER images
A poster of this presentation has been presented in the 5th EARSeL Workshop on Imaging Spectroscopy, Bruges, Belgium, April 2007
A shipwrecked since 1800's

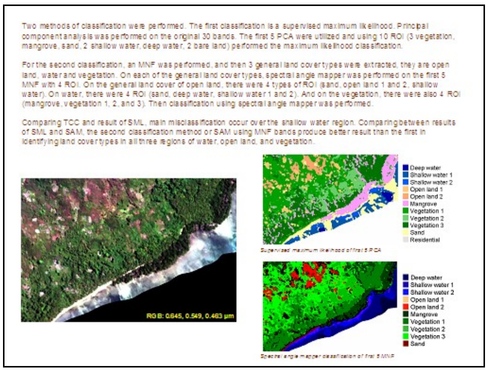
Two methods of classification were performed. The first classification is a supervised maximum likelihood. Principal component analysis was performed on the original 30 bands. The first 5 PCA were utilized and using 10 ROI (3 vegetation, mangrove, sand, 2 shallow water, deep water, 2 bare land) performed the maximum likelihood classification.
For the second classification, an MNF was performed, and then 3 general land cover types were extracted, they are open land, water and vegetation. On each of the general land cover types, spectral angle mapper was performed on the first 5 MNF with 4 ROI. On the general land cover of open land, there were 4 types of ROI (sand, open land 1 and 2, shallow water). On water, there were 4 ROI (sand, deep water, shallow water 1 and 2). And on the vegetation, there were also 4 ROI (mangrove, vegetation 1, 2, and 3). Then classification using spectral angle mapper was performed.
Comparing TCC and result of SML, main misclassification occur over the shallow water region. Comparing between results of SML and SAM, the second classification method or SAM using MNF bands produce better result than the first in identifying land cover types in all three regions of water, open land, and vegetation.
RGB: 0.645, 0.549, 0.463 µm
Deep water
Shallow water 1
Shallow water 2
Open land 1
Open land 2
Mangrove
Vegetation 1
Vegetation 2
Vegetation 3
Sand
Residential
Supervised maximum likelihood of first 5 PCA
Deep water
Shallow water 1
Shallow water 2
Open land 1
Open land 2
Mangrove
Vegetation 1
Vegetation 2
Vegetation 3
Sand
Spectral angle mapper classification of first 5 MNF

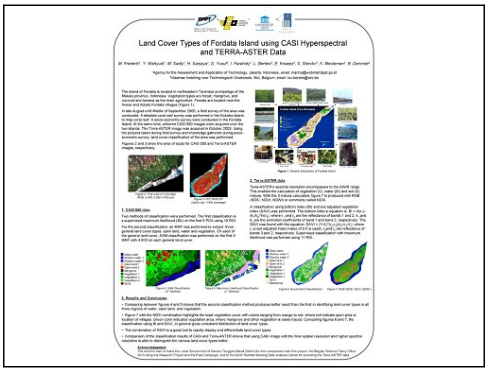
Land Cover Types of Fordata Island using CASI Hyperspectral and TERRA-ASTER Data

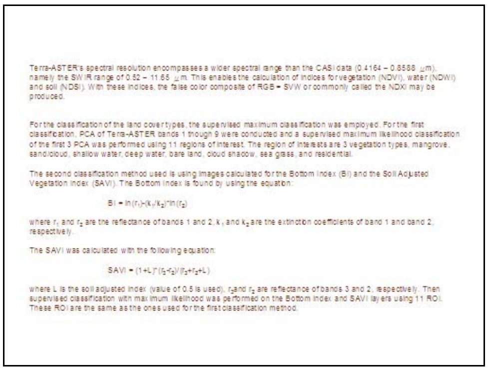
Terra-ASTER's spectral resolution encompasses a wider spectral range than the CASI data (0.4164 – 0.8588 µm), namely the SWIR range of 0.52 – 11.65 µm. This enables the calculation of indices for vegetation (NDVI), water (NDWI) and soil (NDSI). With these indices, the false color composite of RGB = SVW or commonly called the NDXI may be produced.
For the classification of the land cover types, the supervised maximum classification was employed. For the first classification, PCA of Terra-ASTER bands 1 though 9 were conducted and a supervised maximum likelihood classification of the first 3 PCA was performed using 11 regions of interest. The region of interests are 3 vegetation types, mangrove, sand/cloud, shallow water, deep water, bare land, cloud shadow, sea grass, and residential.
The second classification method used is using images calculated for the Bottom Index (BI) and the Soil Adjusted Vegetation Index (SAVI). The Bottom Index is found by using the equation:
BI = ln(r1)-(k1/k2)*ln(r2)
where r1 and r2 are the reflectance of bands 1 and 2, k1 and k2 are the extinction coefficients of band 1 and band 2, respectively.
The SAVI was calculated with the following equation:
SAVI = (1+L)*(r3-r2)/(r3+r2+L)
where L is the soil adjusted index (value of 0.5 is used), r3 and r2 are reflectance of bands 3 and 2, respectively. Then supervised classification with maximum likelihood was performed on the Bottom Index and SAVI layers using 11 ROI. These ROI are the same as the ones used for the first classification method.


Thank you!

Observations of SST and Chlorophyll-a Concentration in Coastal Sea of Vietnam Using Ocean Color Remote Sensing

Tu Tuyet Hong and Nguyen Phi Khu
University Technical Education -HCMC
Vietnam National University - HCMC

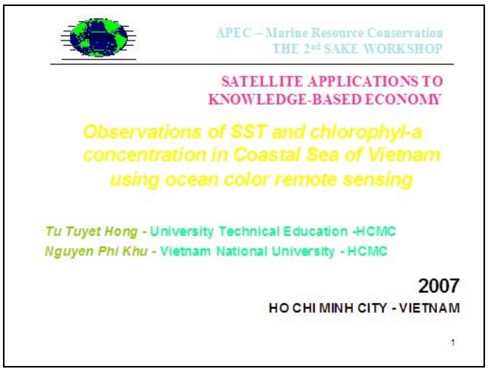

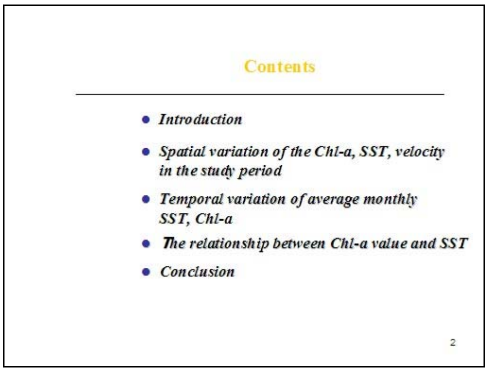

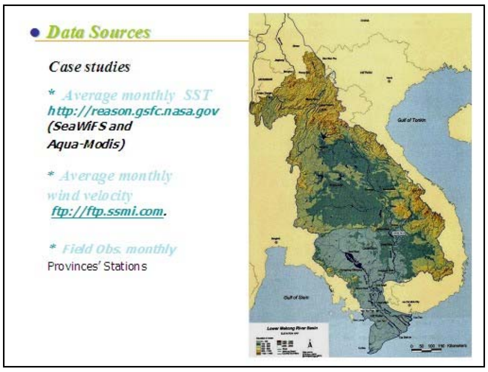

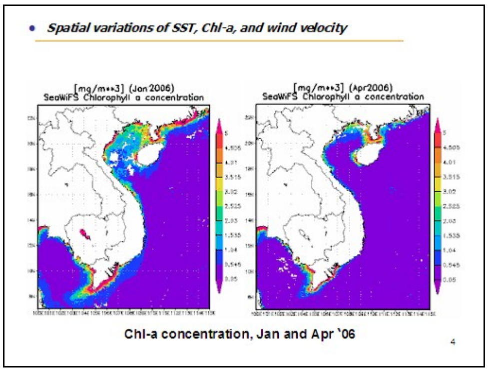

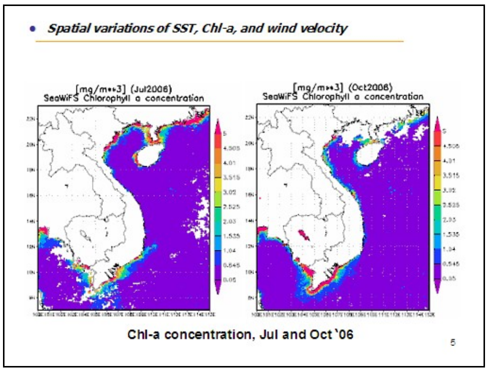

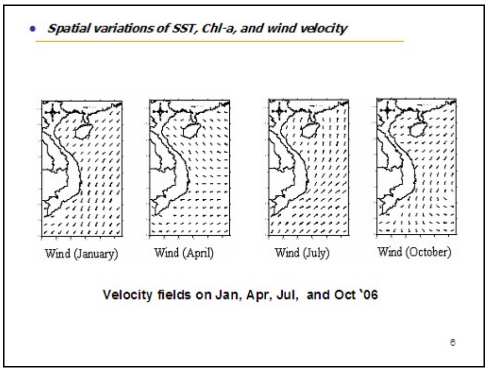

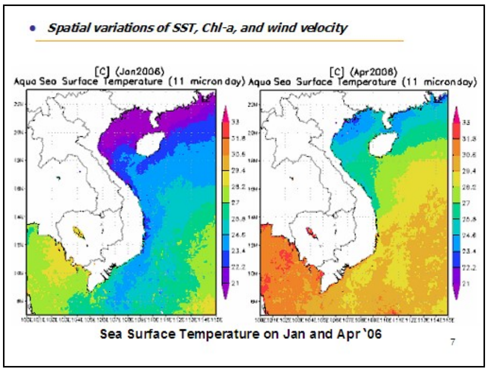

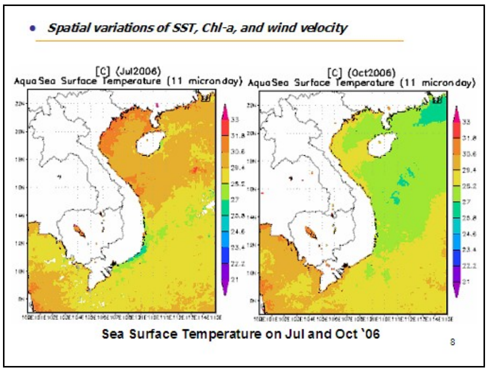

Temporal variation of average monthly SST, Chl-a

Case study: Binh Thuan Province

Time series of Chl-a at Binh Thuan Province in SWM

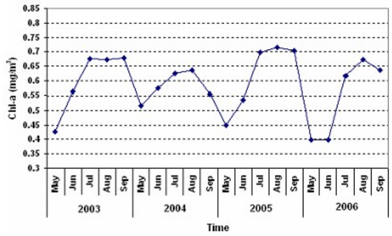

9

- ***Temporal variation of average monthly SST, Chl-a***

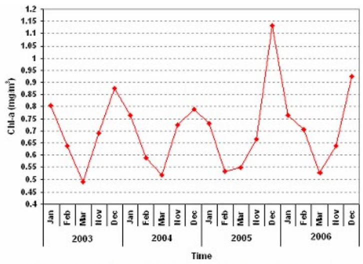

Time series of Chl-a at Binh Thuan Province in NEM

10

- ***The relationship between Chl-a value and SST***

R = 0.907

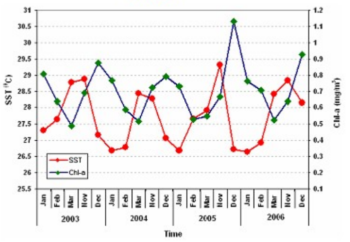

The relationship between SST and Chl-a in NEM season at Binh thuan coastal

11

- ***The relationship between Chl-a value and SST***

Chl-a

	2003	2004	2005	2006
Jan	0.805956	0.764605	0.729043	0.764332
Feb	0.638264	0.589655	0.531317	0.707170
Mar	0.490580	0.517036	0.548989	0.526767
Apr	0.398628	0.400108	0.440129	0.388418
May	0.426313	0.516784	0.450032	0.398820
Jun	0.565014	0.575720	0.536319	0.398655
Jul	0.675098	0.625395	0.697992	0.617969
Aug	0.672159	0.636596	0.716033	0.672409
Sep	0.678790	0.556515	0.705443	0.638000
Oct	0.747492	0.673670	0.600371	0.697513
Nov	0.689427	0.723766	0.667040	0.638014
Dec	0.875886	0.790421	1.130850	0.926213

Selected averaging area: lat=[7.0N,12.0N], lon=[100.0E,110.0E]

The relationship between SST and Chl-a in NEM season at Binh thuan coastal

12

- ***The relationship between Chl-a value and SST***

R = 0.879

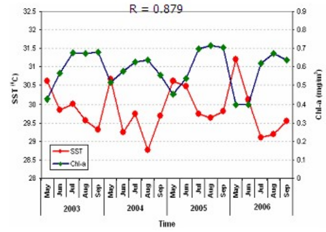

The relationship between SST and Chl-a in SWM season at Binh thuan coastal

13

- ***The relationship between Chl-a value and SST***

SST

	2003	2004	2005	2006
Jan	27.303	26.680	26.685	26.651
Feb	27.651	26.777	27.658	26.935
Mar	28.766	28.440	27.936	28.401
Apr	30.359	29.988	29.762	30.483
May	30.611	30.665	30.615	31.208
Jun	29.858	29.254	30.468	30.117
Jul	30.014	29.741	29.737	29.110
Aug	29.574	28.768	29.632	29.190
Sep	29.323	29.683	29.822	29.553
Oct	29.007	29.028	29.798	29.335
Nov	28.871	28.280	29.318	28.841
Dec	27.160	27.068	26.733	28.158

Averaging area: lat=[7.0N,12.0N], lon=[100.0E,110.0E]

The relationship between SST and Chl-a in SWM season at Binh thuan coastal

14

Recommendation

- ***Spatial distribution features of SST and Chl-a in the Vietnam Sea depend up on: monsoons, precipitation, river runoff, upwelling, ect.***
- ***Temporal variation features of SST and Chl-a indicated that there are 4 seasons at Vietnam Sea: NE monsoon, Transition period from Spring to Summer, SW monsoon, and Transition period from Summer to Winter.***
- ***Along southern Vietnamese coast was formed a nearshore strip of low SST and high Chl-a during SW monsoon period.***
- ***Seasonal Chl-a variation in Vietnam waters is different between the north of Vietnam and south of Vietnam. The central of Vietnam waters is the lowest Chl-a concentration in both two seasons.***
- ***This study found that high Chl-a concentration at south of Vietnam waters from July to September during SWM (> 0.65 mg/m³).***

15

16